Hyperspectral Prediction Model for Mixed Salts on the Surfaces of Temple Murals in Northern China Based on Simulated Samples

Silei Li [1,2], Shuqiang Lyu [1,2], Miaole Hou [1,2], Wenxuan Lin [1,2], Fanyi Meng [1,2]

[1] School of Geomatics and Urban Spatial Informatics, Beijing University of Civil Engineering and Architecture, No.15 Yongyuan Road, Daxing District, 102616 Beijing, China - 2108570023098@stu.bucea.edu.cn; lvshuqiang@bucea.edu.cn; houmiaole@bucea.edu.cn; 2108570424046@stu.bucea.edu.cn; 201904010313@stu.bucea.edu.cn.
[2] Beijing Key Laboratory for Architectural Heritage Fine Reconstruction & Health Monitoring, No.15 Yongyuan Road, Daxing District, 102616 Beijing, China

Keywords: Temple Murals, Mixed Soluble Salt, Hyperspectral, Regression, Multiple Linear Stepwise Regression

Abstract

Murals are invaluable treasures of human civilization, yet they face irreversible damage from salt migration and crystallization caused by environmental fluctuations. This study develops a hyperspectral approach to monitor common salts (anhydrous sodium sulfate (Na_2SO_4) and anhydrous calcium chloride ($CaCl_2$)) on mural surfaces. Using an ASD-FieldSpec4 spectrometer, we analyze simulated mural samples with varying salt concentrations. For data correction, spectral preprocessing was conducted using Savitzky-Golay smoothing (SG), Standard Normal Variate (SNV), and Multiplicative Scatter Correction (MSC). Additionally, the natural logarithm (NL) transformation was introduced and combined with spectral preprocessing to enhance spectral features. The Competitive Adaptive Reweighted Sampling (CARS) algorithm selected characteristic wavelengths, and the Savitzky-Golay-Natural Logarithm-Multiple Linear Stepwise Regression model demonstrated the best predictive capability. For Na_2SO_4 prediction, the model achieved optimal performance with an R^2 of 0.934 and an RMSE of 0.0678% using characteristic bands at 550 nm, 560 nm, 817 nm, 1318 nm, and 1911-2349 nm. For $CaCl_2$ detection, it showed excellent accuracy with an R^2 of 0.987 and an RMSE of 0.0162% at key bands of 404-448 nm, 812 nm, 1137 nm, 1314-1333 nm, and 1922-2465 nm. We predicted multiple salt concentrations on the simulated temple murals using a method based on the NL and the CARS algorithm. We demonstrate a technical approach for hyperspectral detection of mixed salts on the surfaces of typical temple murals in northern China.

1. Introduction

Murals are one of the oldest forms of painting and have an extensive social impact both in China and other countries (Shang, 2009). Murals were prevalent in Chinese temples. However, due to the impact of environmental and anthropogenic factors, the preservation status of murals is far from optimistic. Among various mural diseases, disruption has always been one of the most common and severe problems. Extensive research has demonstrated that disruption is caused by the migration of soluble salts in the plaster layer to the mural surface along with capillary water movement (Wang and Yu, 2010). These salts then repeatedly dissolve, crystallize, expand, and contract with changes in environmental temperature and humidity, which disrupts the structure of the plaster layer and leads to a loose state. Once salt damage occurs, it can cause permanent damage to murals (Xu, 2023). Therefore, developing rapid and effective methods for salt detection on mural surfaces, targeting the predominant salt types, is imperative for conservation efforts.

Recent studies on mural conservation have revealed significant insights into salt-induced deterioration mechanisms. Research conducted at the Mogao Grottoes in Gansu Province, China, demonstrated that SO_4^{2-}-Cl^--Ca^{2+}-Na^+ ionic compounds are primarily responsible for various deterioration patterns including blistering, flaking, and paint loss (Wang, 2010). Subsequent simulation tests further confirmed the particularly damaging effects of Na_2SO_4, showing its exceptional penetration, migration, and crystallization capacities that critically weaken the gritstone matrix (Jin, 2015). These studies established that mixed salt formations constitute the predominant threat to mural integrity (Wang, 2010; Jin et al., 2015).

Contemporary analytical approaches have significantly advanced our understanding of salt composition. Through ion chromatography analysis, predominant anions (SO_4^{2-}, NO_3^-, Cl^-) and cations (K^+, Mg^{2+}) were identified in the murals of Fengguo Temple, Liaoning Province, China (Wei and Liu, 2018). Comprehensive characterization using SEM-EDS and X-ray Diffraction techniques in Mogao Cave 196 (Gansu Province, China) revealed that NaCl and Na_2SO_4 were the primary damaging salts (Zhang, 2021). However, these conventional methods present limitations including high costs, time-consuming procedures, and inability to provide precise concentration measurements for individual components in mixed salt systems (Wei and Liu, 2018; Zhang, 2021).

Hyperspectral technology has emerged as a promising alternative, offering advantages in spectral information richness, sensitivity, and multi-component detection capability (Knyazikhin, 2013; Su, 2021; Gila, 2024; Thorat, 2023). Preliminary applications in mural conservation have shown potential through various modeling approaches. Spectral preprocessing and mathematical transformations enabled the development of regression models (linear, multiple, parabolic) and specialized indices for Na_2SO_4 concentration prediction (Guo, 2023b). Machine learning techniques including Support Vector Machine (SVM), Random Forest (RF), and Partial Least Squares Regression (PLSR) have been successfully implemented for salt content regression (Guo, 2023a). Advanced methodologies incorporating fractional-order differentiation with PLSR modeling demonstrated effectiveness in phosphate prediction (Ren, 2024a), while three-band detection methods based on photochemical reflectance indices

showed strong correlations with phosphate content (Ren, 2024b).

This study focused on producing high-fidelity simulated mural replicas that replicate the structural composition and salt typology characteristic of temple murals in northern China. By preparing simulation samples containing different concentrations of Na_2SO_4 and $CaCl_2$, we collected the spectral reflectance of the samples using an ASD-FieldSpec4HI-RES spectrometer. Then, Savitzky- Golay (SG), Standard Normal Variate (SNV), and Multiplicative Scatter Correction (MSC) were used for spectral preprocessing. We proposed a method of enhancing spectral features through natural logarithm (NL) operation and used Competitive Adaptive Reweighted Sampling (CARS) for feature band selection. Finally, a multiple linear stepwise regression (MLSR) model was established. The results demonstrate that the spectral data processed by SG and NL operation can better predict the content of mixed salts. The model has strong prediction ability and good stability. This study is of great significance for the detection of mixed salts on the surface of temple murals in northern China and provides a new technical idea for the salt detection on the surface of real murals.

2. Data Acquisition and Preprocessing

2.1 Sample Preparation and Data Collection

Based on the production process of temple murals in northern China (Jin, 2023; Yao, 2023), we made mural simulation samples in the laboratory. The samples mainly consisted of a coarse plaster and a fine plaster. Since salt damage primarily results from salt crystallization on the mural surface, the soluble salt content was defined as the mass ratio of salts to dry fine plaster. Based on analysis of salt types and concentrations from real temple murals, simulation samples were prepared with varying concentrations of Na_2SO_4 (predominant) and $CaCl_2$. Some of the prepared samples are shown in Figure 1.

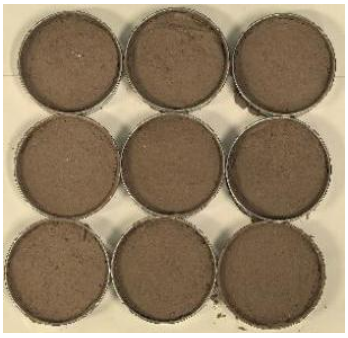

Figure 1. Simulated samples of mixed salts for the murals in temples in northern China

After preparation, the samples were placed in the laboratory to dry in the shade, and then their surfaces were scraped flat. Then, the reflectance spectra of the samples were collected using an ASD-FieldSpec4HI-RES spectrometer. The specific parameters of this instrument are shown in Table 1. The data collection was carried out in a darkroom, with a halogen lamp as the only light source. The probe was perpendicular to the sample. Four curves were collected from different positions of each sample each time. After breakpoint correction, the average value of the reflectance spectra was recorded as the data result of this measurement. The spectral data were collected every 24 hours, and a total of 72 sample reflectance spectra were obtained.

Parameter Name	Specific values
Product model	FieldSpec4HI-Res
Spectral range	350-2500nm
Spectral resolution	3nm @ 700nm 8nm @ 1400/2100nm
Sampling interval	1.4nm @ 350-1000nm 1.1nm @ 1001-2500nm
Number of channels	2151

Table 1. Technical specifications of the ASD-FieldSpec4HI-RES spectrometer used for reflectance measurements.

2.2 Data Preprocessing

During the data acquisition process, noise may be generated due to factors such as the instrument itself, human factors, and the environment. To effectively reduce the interference of noise on the research results, breakpoint correction was first carried out on the collected data to eliminate the systematic error caused by the differences in the characteristics of different optical components inside the instrument. In addition, to avoid errors caused by human factors during the measurement process, for each sample, four different positions were selected for measurement, and the obtained spectral data were averaged and used as the final measurement result. Secondly, spectral preprocessing was carried out using SG smoothing, SNV, and MSC. SG smoothing can effectively reduce the noise in the spectrum and improve the quality and stability of the signal by fitting the spectral data with a polynomial (Ochieng, 2023). SNV normalizes the spectrum by subtracting the mean value from each spectral data point and dividing it by the standard deviation. It can eliminate scattering effects such as baseline offset and slope change in the spectral data, making the spectra of different samples comparable in intensity and highlighting the characteristic differences of the spectra (Shi, 2021). MSC minimizes the wavelength-related multiplicative deviation caused by light scattering by fitting a linear model between the reference spectrum and other spectra in the dataset (Centner, 2000).

3. Methods

To achieve the detection of mixed salts on the surface of typical temple murals in northern China, we established the technical process shown in Figure 2.

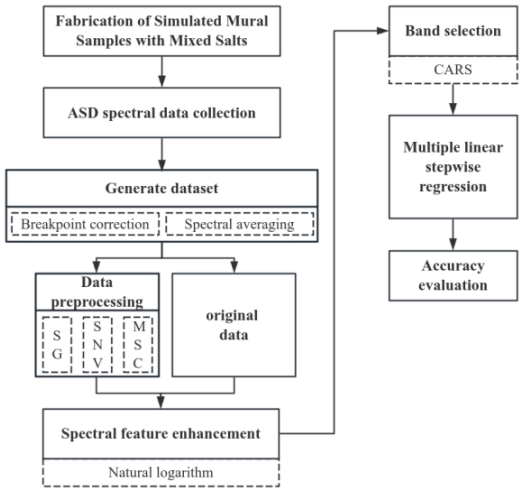

Figure 2. Flow Chart of the Detection of the Content of Mixed Salts on the Surface of Murals in Northern China

First, after preparing the simulated mural samples, the spectral data of the samples were collected using an ASD-FieldSpec4HI-RES spectrometer. Then, we performed breakpoint correction and spectral averaging to form a model dataset. And three preprocessing operations, SG smoothing, SNV, and MSC, were carried out on the spectral data to reduce the deviation of the spectral data. Then, we calculated the NL to enhance the spectral features and used CARS to select the band combinations highly correlated with the concentrations of the two types of salts. Finally, a MLSR was used to establish a prediction model for mixed salts, and the accuracy of the model was comprehensively evaluated based on the coefficient of determination and the root mean square error.

3.1 Spectral Feature Enhancement

In order to highlight spectral differences, reflect subtle changes, eliminate interference such as noise and baseline drift, and thus improve the accuracy of information extraction and enhance data separability, we used mathematical operations for spectral feature enhancement (Louchard, 2002; Wang, 2020). Research has demonstrated that logarithmic transformation provides the optimal spectral transformation for predicting soil organic matter content using hyperspectral data (Guo et al., 2024). Logarithmic transformation can suppress background noise, highlight the absorption peaks of data, and enhance the differences between spectral data, thereby reducing errors in the data and enhancing the data.

3.2 Feature Band Selection

Due to the continuity of hyperspectral data, the enhanced spectral data still contain redundant information, which will affect the efficiency of the prediction model. Therefore, the competitive adaptive reweighted sampling algorithm was used to select the optimal band combination for model establishment. CARS is a band selection method based on Monte Carlo sampling. This algorithm screens out the bands highly correlated with the target variable through exponentially decaying weights. In this way, it can effectively reduce redundant information, improve the accuracy of the model, and increase the operation efficiency (Fan, 2012). The integration of PLSR with competitive adaptive reweighted sampling (CARS) has been shown to effectively select key variables containing the most significant information. Comparative results demonstrated that the CARS-PLSR method achieved significantly greater accuracy than conventional full-spectrum PLSR analysis. Following band selection, the predictive capability of spectral data for salt content determination was markedly enhanced while simultaneously reducing data redundancy (Vohland et al., 2014). We used the absolute value of PLSR coefficients to determine the importance of variables, and achieved a smooth transition through an exponential decay function to retain variables with high weights.

3.3 Prediction Model and Accuracy Evaluation

MLSR is a statistical method that screens independent variables according to specific rules during the establishment of a multiple regression equation. It ensures that the final model contains only the independent variables that have a significant impact on the dependent variable and have no serious multicollinearity. By gradually introducing and eliminating variables, it can obtain the optimal regression equation (Kabe, 1963; Grossman, 1996). Several modeling approaches including MLSR, PLSR, and SVM have been successfully applied to estimate total nitrogen content in soil (Shi et al., 2013). The established models were comprehensively evaluated using the coefficient of determination (R^2) and the root mean square error (RMSE). Among them, R^2 is used to measure the goodness of fit of the model to the data. The value range of R^2 is between 0 and 1. The closer R^2 is to 1, the stronger the explanatory power of the independent variables for the dependent variable (Ozer, 1985). RMSE is mainly used to evaluate the average error degree between the predicted values and the true values of the model. The smaller the RMSE value, the closer the predicted values are to the true values, indicating a stronger prediction ability of the model (Hodson, 2022).

4. Results and Analysis

4.1 Spectral Feature Analysis of Mural Simulation Samples with Mixed Salts

The original spectrum of the simulation sample is shown in Figure 3(a). The spectral curve is relatively smooth, lacking severe jumps or sharp peaks and valleys. This smoothness indicates that the light reflection characteristics of the simulation sample change continuously across the entire wavelength range, with no sudden changes in very narrow bands. In the wavelength range from 500nm to 2500nm, the reflectance of the simulation sample first increases, then tends to be stable, and then shows a small amplitude fluctuating decrease in specific bands. Near 500nm, the reflectance is low. As the wavelength increases, the reflectance gradually increases and tends to be stable between about 1000 - 1500nm. Then, there are some small peaks and valleys near 2000nm, and finally, the reflectance decreases near 2500nm.

The data after preprocessing are presented in Figures 3 (b - d), demonstrating the results of different preprocessing methods. After SG smoothing, the curve becomes smoother, with small fluctuations weakened or eliminated, thereby highlighting the detailed features of the spectrum. After SNV processing, the differences among spectral curves become more pronounced, particularly in bands with relatively sharp peaks or valleys. After MSC processing, the spectral curve shows greater regularity compared to the original spectrum. Moreover, the degree of dispersion between the curves decreases, effectively eliminating the influence of the differences in the physical properties of the sample surface on the spectrum. As shown in Figure 3(e), after the NL transformation, the spectral curve changes more sensitively in the low reflectance region, while the changes in the high reflectance region are relatively gentle. Compared with the original spectrum, the overall dynamic range is compressed.

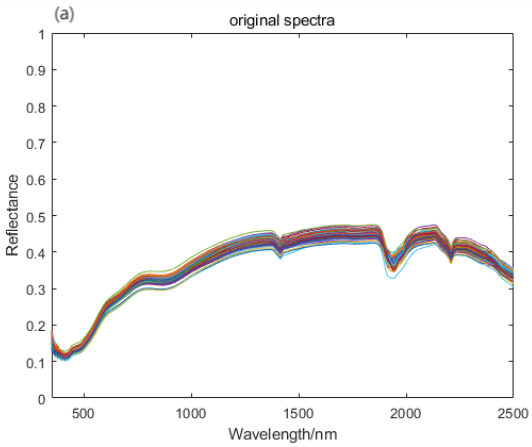

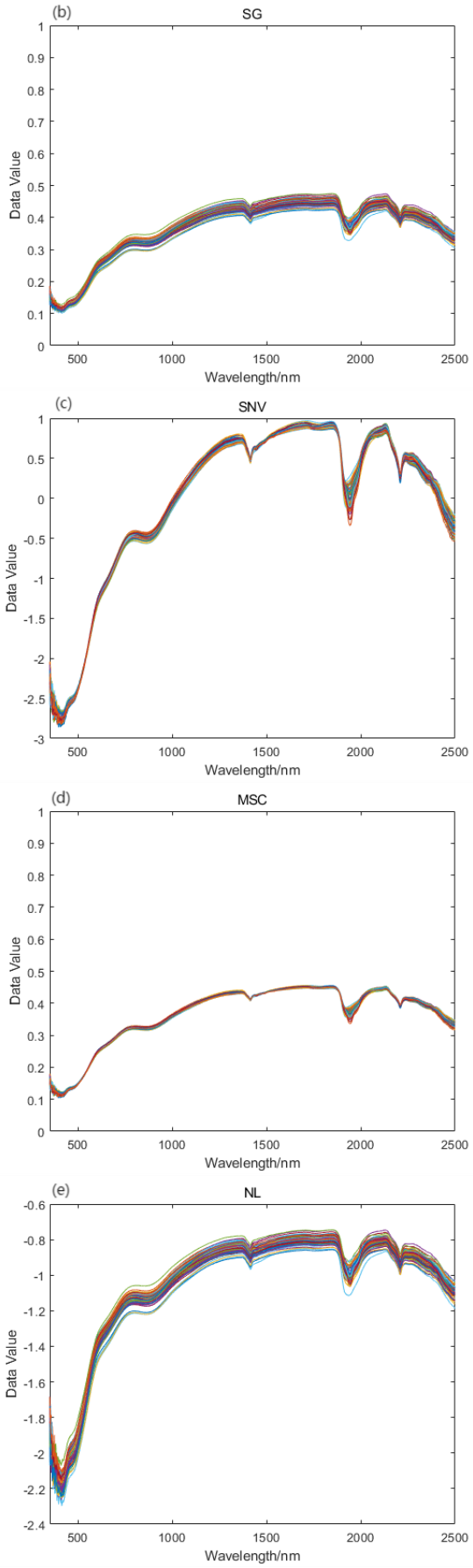

Figure 3. Mural simulated sample (a)Original spectrum (b)SG (c)SNV (d)MSC (e)NL

We applied the CARS method to perform feature band selection on the original spectral data and the preprocessed spectral data, and respectively selected the band combinations highly correlated with the concentrations of the two types of salts. The selected band combinations are presented in Table 2.

Data form	Optimal Band Combination(nm)	
	Na_2SO_4	$CaCl_2$
R	377、387、409、423、846、852、1309、2144、2309	366、409、834、1325、1908、1947、1953、2133、2417、2486
SG	387、867、1921、1927、2080、2156 2257、2309、2311	436、810、1325、1912、1974、2134、2453
SNV	367、381、386、870、878、1918、1928、1946、1954、2092、2364	350、390、1279、1914、1975、2423
MSC	350、352、353、 371、392、443、2154、2158、2162、2308、2366、2372	352、404、444、1914、1975、1977、2151、2446
NL	392、423、430、436、529、1161、1920、1922、1952、2086、2087、2308	387、412、448、810、823、825、1139、1905、1909、1963、1971、2422
SG-NL	550、560、817、1318、1911、1912、1924、2044、2349	404、428、444、448、812、1137、1314、1333、1922、1973、1975、1976、2133、2144、2465

Table 2. Optimal band combinations for different salt components

4.2 Accuracy Analysis of MLSR

We used the feature band combinations selected by CARS in Table 2 as independent variables and input them into the MLSR model. The accuracy of the established models and the regression equations is shown in Table 3 and Table 4. The selected bands provide more concise and useful information, effectively avoiding the presence of redundant information that could otherwise complicate the analysis. The accuracy of all models exceeds 0.865, meeting the requirement for high-accuracy salt prediction using fewer bands. In the prediction of Na_2SO_4, the R^2 is mostly above 0.9, and the RMSE is mostly in the range of 0.0678% - 0.0803%. A higher R^2 indicates that the model can explain most of the changes in the sodium sulfate content. Meanwhile, a lower RMSE indicates that the predicted values are relatively close to the true values, suggesting good overall prediction accuracy. The SG - NL model composed of bands of 550nm, 560nm, 817nm, 1318nm, 1911nm, 1912nm, 1924nm, 2044nm, and 2349nm has the highest accuracy, with a R^2 of 0.934 and a RMSE of 0.0678%. In the prediction of $CaCl_2$, R^2 is in the range of 0.865 - 0.987, and RMSE is in the range of 0.0162% - 0.0478%. The model composed of bands of 404nm, 428nm, 444nm, 448nm, 812nm, 1137nm, 1314nm, 1333nm, 1922nm, 1973nm, 1975nm, 1976nm, 2133nm, 2144nm, and 2465nm has the highest accuracy, with a R^2 of 0.987 and a RMSE of 0.0162%. Considering the prediction results of the two types of salts, the SG - NL model has the highest accuracy. This result may be attributed to the combination of SG smoothing and NL transformation, which reduces the redundant information and

noise interference in the data to a certain extent. Among the established models, except for the $CaCl_2$ model established by SNV, all models show relatively high prediction accuracy, providing a new way to solve the problem of predicting the content of mixed salts on the surface of murals.

Figure 4 presents the scatter plots of the prediction results for Na_2SO_4 and $CaCl_2$, illustrating the linear relationship between predicted and actual values. From the scatter point distribution, the points in each plot roughly follow the linear trend line. In the low concentration range, the scatter points of most models are comparatively closer to the prediction fitting line, the distribution of the scatter points is fairly uniform, and the scatter points are rather concentrated near the fitting line, indicating that the models have relatively accurate predictions in the low concentration range. However, at high concentration levels, some data points are quite scattered, and the vertical distance from the fitting line is considerably far, which implies that the prediction performance of the models is average at high concentrations.

Nevertheless, despite some limitations at high concentrations, these models still provide significant reference value for relevant analysis and prediction. Overall, models with different processing methods have their own pros and cons in various concentration ranges, yet they can collectively offer valuable insights for the research. However, in the regression prediction of $CaCl_2$, the scatter points of the model processed by SNV are relatively more scattered, and the prediction accuracy of this model is poor.

Data form	Variable number	Fitting the model equation	R^2	RMSE (%)
R	9	$y=-6.63333R_{377}-12.50975R_{387}+26.77414R_{409}+30.88221R_{423}-752.19775R_{846}+698.49994R_{852}+48.82401R_{1309}-115.80321R_{2144}+111.35878R_{2309}-1.15971$	0.907	0.0803
SG	9	$y=37.04454R_{387}-77.15374R_{867}+71.34211R_{1921}+22.64951R_{1927}-14.88896R_{2080}-91.28568R_{2156}+62.31931R_{2257}-54.69365R_{2309}+71.31349R_{2311}-3.09089$	0.924	0.0727
SNV	11	$y=-0.71124R_{367}-0.68592R_{381}-0.80713R_{386}+42.72285R_{870}-46.67742R_{878}-23.24119R_{1918}+41.88082R_{1928}-12.42043R_{1946}-7.86589R_{1954}-7.40115R_{2092}+3.22527R_{2364}-0.742571$	0.916	0.0776
MSC	11	$y=-4.01388R_{350}+10.33110R_{352}-4.17696R_{353}+12.57339R_{371}-15.24410R_{392}+35.05127R_{443}-515.38795R_{2154}+668.09748R_{2158}-321.01912R_{2162}+110.03725R_{2308}-168.59557R_{2366}+171.06609R_{2372}+24.2078$	0.928	0.0725
NL	12	$y=-1.97544R_{392}+4.48894R_{423}+4.66277R_{430}+5.71620R_{436}-15.21777R_{529}+5.34497R_{1161}-174.85140R_{1920}+196.02883R_{1922}-22.51131R_{1952}-517.24834R_{2086}+498.72359R_{2087}+19.45448R_{2308}+7.05601$	0.931	0.0709
SG-NL	9	$y=125.80112R_{550}-128.45399R_{560}-20.90049R_{817}+34.84576R_{1318}-329.65981R_{1911}+364.99146R_{1912}-25.06175R_{1924}-47.65002R_{2044}+27.575882R_{2349}+5.85827$	0.934	0.0678

Table 3. Results of the model for the content of sodium sulfate in the simulated mural sample

Data form	Variable number	Fitting the model equation	R^2	RMSE (%)
R	10	$y=-4.21595R_{366}+16.74013R_{409}-24.06319R_{834}+23.538889R_{1325}+19.42225R_{1908}+51.637794R_{1947}-81.54476R_{1953}-26.48231R_{2133}+21.15948R_{2417}+14.21843R_{2486}-0.529364$	0.931	0.0353
SG	7	$y=19.85252R_{436}-39.88647R_{810}+38.99704R_{1325}+20.07128R_{1912}-33.38406R_{1974}-22.84239R_{2134}+30.90901R_{2453}-1.52188$	0.965	0.0246
SNV	6	$y=-0.21346R_{350}+0.424214R_{390}+3.08578R_{1279}+2.43760R_{1914}-2.85930R_{1975}+2.452096R_{2423}-0.891151$	0.865	0.0478
MSC	8	$y=2.22820R_{352}-12.87180R_{404}+33.32963R_{444}+20.18367R_{1914}+138.01858R_{1975}-178.87871R_{1977}-51.481209R_{2151}+36.44494R_{2446}+15.2191$	0.956	0.0277
NL	12	$y=-0.50625R_{387}-0.75472R_{412}+4.52826R_{448}-36.98169R_{810}-134.85333R_{823}+155.99834R_{825}+14.97931R_{1139}-27.107986R_{1905}+32.52513R_{1909}+24.56646R_{1963}-38.21632R_{1971}+7.14051R_{2422}+2.71918$	0.953	0.0297
SG-NL	15	$y=-0.70466R_{404}-4.15010R_{428}+4.49554R_{444}+3.57119R_{448}-17.65851R_{812}+16.03811R_{1137}-68.14684R_{1314}+70.73591R_{1333}+11.80946R_{1922}+66.19807R_{1973}-367.50506R_{1975}+284.23203R_{1976}-33.48425R_{2133}+25.93225R_{2144}+9.249565R_{2465}+2.16246$	0.987	0.0162

Table 4. Results of the model for the content of calcium chloride in the simulated mural sample

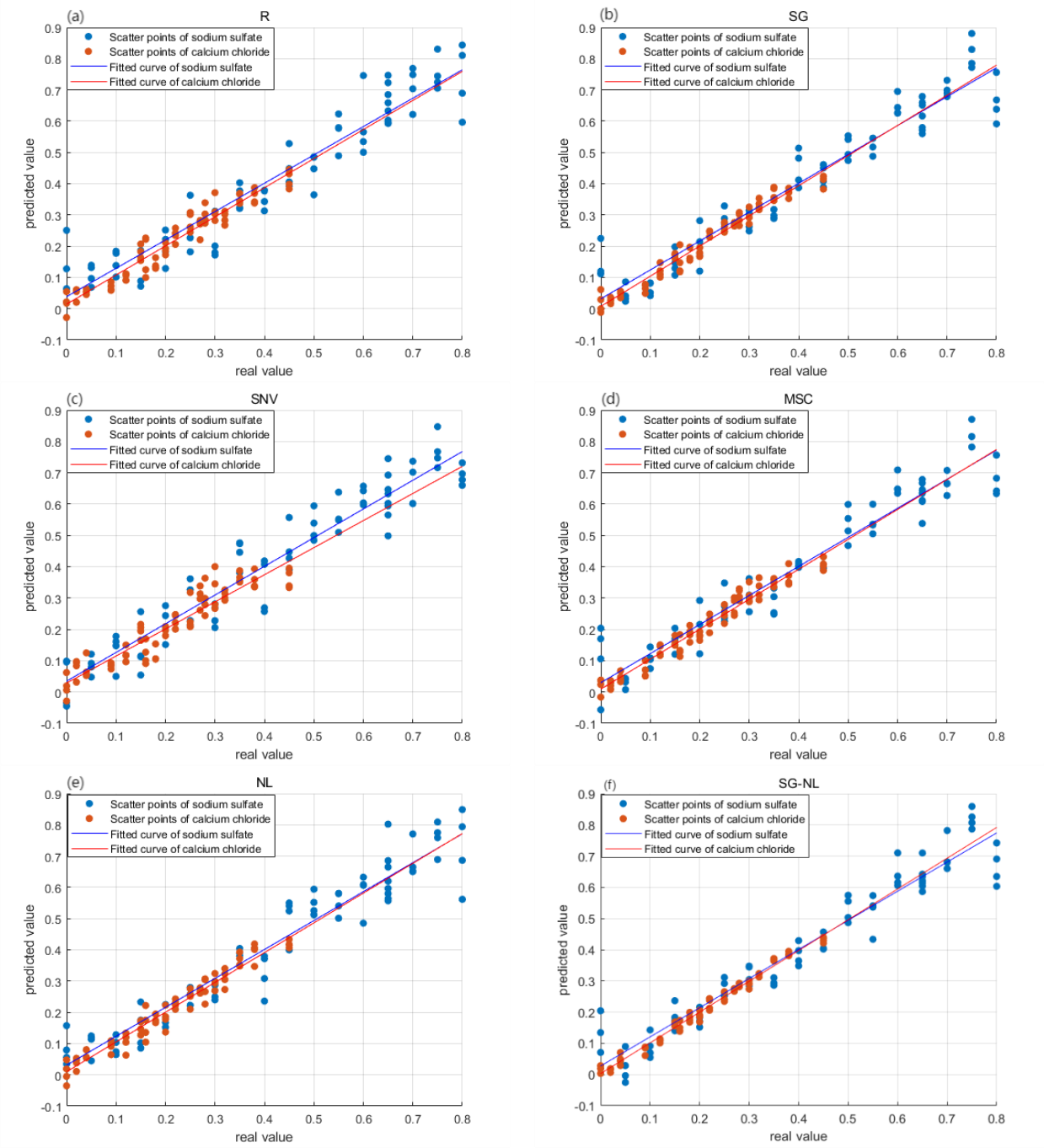

Figure 4. Scatter plot of the prediction model for sodium sulfate and calcium chloride in simulated mural

5. Discussion

MLSR can effectively predict the respective contents of mixed salts in mural simulation samples. A large amount of information in hyperspectral data well reflects the information of salt content. Through data preprocessing and NL operation, the capacity of spectral data to convey meaningful information can be effectively enhanced. The characteristic band combinations extracted by CARS can effectively represent the majority of information contained in hyperspectral data. By this way, it circumvents the issues associated with the vast quantity of hyperspectral data and the resulting slow modeling efficiency. However, a complex non-linear relationship may exist between salt concentration and spectral features, making it difficult for linear models to accurately describe this relationship. The models are extremely sensitive to minor changes in data and have poor generalization ability. Therefore, it is necessary to continue to explore the non - linear relationship between salt concentration and spectral features.

6. Conclusion

We took temple murals in northern China as the research object. We prepared simulated mural samples containing varying concentrations of Na_2SO_4 and $CaCl_2$. The spectral data of these samples were acquired using an ASD-FieldSpec4HI-RES spectrometer. Subsequently, we performed systematic data processing on the obtained spectral datasets. Finally, comprehensive analyses were conducted based on the processed

spectral data. Based on these efforts, the following conclusions were obtained:

It is feasible to perform spectral preprocessing using SG smoothing, SNV, and MSC. Additionally, introducing the NL operation can enhance spectral features. By combining with the CARS algorithm to select characteristic bands, we can establish a MLSR model. This method can effectively extract spectral information related to salt concentration and achieve the prediction of mixed salt content.

The SG - NL - MLSR model established based on the spectral data processed by SG and NL operation has the best prediction ability. When predicting the concentration of Na_2SO_4, the model using a combination of 9 strongly correlated bands (e.g., 550 nm, 560 nm) achieves an R^2 of 0.934 and an RMSE of 0.0678%. When predicting the content of $CaCl_2$, using a combination of 15 strongly correlated bands such as 404nm and 428nm, R^2 is 0.987, and RMSE is 0.0162%. Overall, most models exhibit an accuracy above 0.865, with RMSE mostly ranging from 0.0162% to 0.0803%, thus enabling high-precision salt prediction with fewer bands.

This study provides a new technical idea for the detection of mixed salts on the surface of temple murals in northern China and is of great significance for the salt detection on the surface of real murals.

Acknowledgements

This work was supported by the Open Project of the Chinese Academy of Cultural Heritage, "Salt Spectral Response Mechanism and Quantitative Retrieval Method of Typical Temple Murals - Taking Cheng'en Temple in Beijing and Yiju Temple in Shanxi Province as Examples". It was also supported by the National Natural Science Foundation of China (No.42171356 and No.42171444).

References

Centner, V., Verdú-Andrés, J., Walczak, B., Jouan-Rimbaud, D., Despagne, F., Pasti, L., Poppi, R., Massart, D., & De Noord, O. E., 2000: Comparison of multivariate calibrationt echniques applied to experimental NIR data sets. *Appl. Spectrosc.*, 54(4), 608-623. doi.org/10.1366/0003702001949816.

Fan, W., Shan, Y., Li, G., Lv, H., Li, H., & Liang, Y., 2011: Application of competitive adaptive reweighted sampling method to determine effective wavelengths for prediction of total acid of vinegar. *Food Anal. Methods*, 5(3), 585-590. doi.org/10.1007/s12161-011-9285-2.

Gila, D. M. M., Martínez, D. B., Martínez, S. S., Marchal, P. C., & García, J. G., 2024: Non-invasive detection of pesticide residues in freshly harvested olives using hyperspectral imaging technology. *Smart Agric. Technol.*, 9, 100644. doi.org/10.1016/j.atech.2024.100644.

Grossman, Y., Ustin, S., Jacquemoud, S., Sanderson, E., Schmuck, G., & Verdebout, J., 1996: Critique of stepwise multiple linear regression for the extraction of leaf biochemistry information from leaf reflectance data. *Remote Sens. Environ.*, 56(3), 182-193. doi.org/10.1016/0034-4257(95)00235-9.

Guo, P., Li, M. Y., Zhao, Y., Sun, Z., Chen, X. W., & Li, T., 2024: Performance of hyperspectral data in predicting and map soil organic matter content. In *IGARSS 2024*, 5175-5178. doi.org/10.1109/IGARSS53475.2024.10640391.

Guo, Z.Q., Lyu, S.Q., & Hou, M.L., 2023a: Estimation of the soluble salt concentration in murals based on spectral transformation and feature extraction modelling. *J. Appl. Spectrosc.*, 90(5), 1123-1132. doi.org/10.1007/s10812-023-01642-3.

Guo, Z.Q., Lyu, S.Q., Hou, M.L., Sun, Y.T., Li, S.Y., & Cui, W.Y., 2023b: Inversion of salt content in simulated mural based on hyperspectral mural salt index. *Spectrosc. Spect. Anal.*, 43(10), 3272-3279. doi.org/10.3964/j.issn.1000-0593(2023)10-3272-08.

Hodson, T.O., 2022: Root-mean-square error (RMSE) or mean absolute error (MAE): When to use them or not. *Geosci. Model Dev.*, 15(14), 5481–5487. doi.org/10.5194/gmd-15-5481-2022.

Jin, C., Guo, H., Yu, H.K., Li, B., Yang, J.D., & Zhang, Y., 2023: Spectral analysis of the techniques and material used to make murals - a case study of the murals in Huapen Guandi Temple in Yanqing District, Beijing. *Spectrosc. Spect. Anal.*, 43(4), 1147-1154. doi.org/10.3964/j.issn.1000-0593(2023)04-1147-08.

Jin, Z.L., Chen, G.Q., Xia, Y., Su, B.M., Zhou, T., & Lyu, G.X., 2015: Comparative study of salt damage caused by sulfates and chlorides to mural paintings - evidence of superpenetration, migration and crystallization destruction resulting from sodium sulfate. *Sci. Conserv. Archaeol.*, 27(1), 29-38. doi.org/10.16334/j.cnki.cn31-1652/k.2015.01.005.

Kabe, D.G., 1963: Stepwise multivariate linear regression. *J. Am. Stat. Assoc.*, 58(303), 770-773. doi.org/10.1080/01621459.1963.10500886.

Knyazikhin, Y., Schull, M. A., Stenberg, P., Mõttus, M., Rautiainen, M., Yang, Y., Marshak, A., Carmona, P. L., Kaufmann, R. K., Lewis, P., Disney, M. I., Vanderbilt, V., Davis, A. B., Baret, F., Jacquemoud, S., Lyapustin, A., & Myneni, R. B., 2012: Hyperspectral remote sensing of foliar nitrogen content. *Proc. Natl. Acad. Sci. USA*, 110(3), E185-E192. doi.org/10.1073/pnas.1210196109.

Louchard, E., Reid, R., Stephens, C., Davis, C., Leathers, R., Downes, T., & Maffione, R., 2002: Derivative analysis of absorption features in hyperspectral remote sensing data of carbonate sediments. *Opt. Express*, 10(26), 1573-1584. doi.org/10.1364/oe.10.001573.

Ochieng, P. J., Maróti, Z., Dombi, J., Krész, M., Békési, J., & Kalmár, T., 2023: Adaptive Savitzky-Golay filters for analysis of copy number variation peaks from whole-exome sequencing data. *Information*, 14(2), 128. doi.org/10.3390/info14020128.

Ozer, D.J., 1985: Correlation and the coefficient of determination. *Psychol. Bull.*, 97(2), 307-315. doi.org/10.1037/0033-2909.97.2.307.

Ren, Y.K., & Liu, F., 2024a: A model for inversion of hyperspectral characteristics of phosphate content in mural plaster based on fractional-order differential algorithm. *Sci. Rep.*, 14(1), 17898. doi.org/10.1038/s41598-024-68594-2.

Ren, Y.K., & Liu, F., 2024b: The spectral inversion model for electrical conductivity in mural plaster following phosphate

erosion based on fractional order differentiation and novel spectral indices. *Herit. Sci.*, 12(1), 286. doi.org/10.1186/s40494-024-01385-0.

Shang, L.B., 2009: Mural painting technology of traditional Chinese temples. *Archicreation*, (2), 138-145.

Shi, T., Cui, L., Wang, J., Fei, T., Chen, Y., & Wu, G., 2013: Comparison of multivariate methods for estimating soil total nitrogen with visible/near-infrared spectroscopy. *Plant Soil*, 366(1–2), 363-375. doi.org/10.1007/s11104-012-1436-8.

Shi, X., Yao, L., & Pan, T., 2021: Visible and near-infrared spectroscopy with multi-parameters optimization of Savitzky-Golay smoothing applied to rapid analysis of soil Cr content of Pearl River Delta. *J. Geosci. Environ. Prot.*, 9(3), 75-83. doi.org/10.4236/gep.2021.93006.

Su, Z., Zhang, C., Yan, T., Zhu, J., Zeng, Y., Lu, X., Gao, P., Feng, L., He, L., & Fan, L., 2021: Application of hyperspectral imaging for maturity and soluble solids content determination of strawberry with deep learning approaches. *Front. Plant Sci.*, 12, 736334. doi.org/10.3389/fpls.2021.736334.

Thorat, T., Patle, B., Wakchaure, M., & Parihar, L., 2023: Advancements in techniques used for identification of pesticide residue on crops. *J. Nat. Pestic. Res.*, 4, 100031. doi.org/10.1016/j.napere.2023.100031.

Vohland, M., Ludwig, M., Thiele-Bruhn, S., & Ludwig, B., 2014: Determination of soil properties with visible to near-and mid-infrared spectroscopy: Effects of spectral variable selection. *Geoderma*, 223-225, 88-96. doi.org/10.1016/j.geoderma.2014.01.013.

Wang, J.F., Yan, G.S., & Yang, S.L., 2010: Distribution of soluble salts in the cliff strata of the Mogao Grottoes. *Hydrogeol. Eng. Geol.*, 37(6), 116-120. 10.16030/i.cnki.issn.1000-3665.2010.06.006.

Wang, X., Li, Z., Zheng, D., & Wang, W., 2020: Nondestructive identification of millet varieties using hyperspectral imaging technology. *J. Appl. Spectrosc.*, 87(1), 54-61. doi.org/10.1007/s10812-020-00962-y.

Wang, Y.J., Yu, Q.L., Yan, M., Ma, L.Y., & Chen, G.Q., 2010: Research on the mobility of soluble salts for north temple murals. *Sci. Conserv. Archaeol.*, 22(3), 15-20.

Wei, R., & Liu, C., 2018: Investigation and analysis of soluble salts in the architectural murals of Fengguo Temple in Liaoning Province. *Identif. Appreciat. Cult. Relics*, (13), 92-93.

Xu, L.N., Que, Y.Q., Ma, Q., & Zhang, Q., 2023: Overview of research on plaster disruption in murals. *Sci. Conserv. Archaeol.*, 35(6), 124-136. doi.org/10.16334/j.cnki.cn31-1652/k.20221002700.

Yao, Y.X., Huang, Y.Z., Ma, Y., Qi, Y.M., & Wei, S.Y., 2023: The identification and analysis of the materials and workmanship for the Water-and-Land-Murals of Daxiong Dian (Hall) of Princess Temple, Fanshi. *Spectrosc. Spect. Anal.*, 43(4), 1155-1161. doi.org/10.3964/j.issn.1000-0593(2023)04-1155-07.

Zhang, Y.X., Yu, Z.R., Wang, L.Q., Cui, Q., Shui, B.W., & Sun, S.L., 2021: A study on the soluble salts used in the murals of Mogao Cave 196. *Dunhuang Res.*, (1), 148-155. doi.org/10.13584/j.cnki.issn1000-4106.2021.01.02